Molecular charge transport : relating orbital structures to the conductance properties

Guédon, C.M.

4

Interpretation of transition voltage spectroscopy

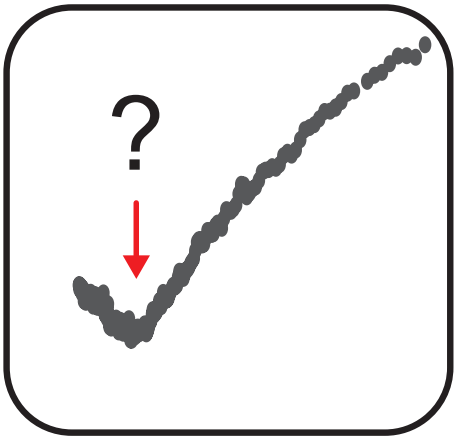

The results presented in this chapter have been published as:

E. H. Huisman, C. M. Guédon, B. J. van Wees and S. J. van der Molen, *Interpretation of Transition Voltage Spectroscopy*, **Nano Letters**, **9**, 3909 (2009)

and

M. L. Trouwborst, C. A. Martin, R. H. M. Smit, C. M. Guédon, T. A. Baart, S. J. van der Molen and J. M. van Ruitenbeek, *Transition Voltage Spectroscopy and the Nature of Vacuum Tunneling*, **Nano Letters**, **11**, 614 (2011)

The promise of 'transition voltage spectroscopy' (TVS) is that molecular level positions can be determined in molecular devices without applying extreme voltages. Here, we consider the physics behind TVS in more detail. Remarkably, we find that the Simmons model employed thus far is inconsistent with experimental data. Moreover we perform experiments on vacuum tunnel junctions to compare to molecular junctions and theory. We show that the promise of TVS is difficult to achieve.

4.1 TRANSITION VOLTAGE SPECTROSCOPY

Over the last decade, several methods have been developed to fundamentally study charge transport in metal-molecule-metal junctions [1–4]. Nevertheless, much of the physics behind molecular transport is still under debate. In fact, simple questions such as "Where does the voltage drop in a molecular junction?" and "Where are the molecular levels with respect to the electrodes' Fermi levels?" have not found general solutions yet. The latter question, for example, is hard to answer experimentally due to the limited voltage a two-terminal molecular junction can withstand. In a molecular device, the Fermi level (E_F) of the metal electrodes is typically a few eV away from the closest molecular level (see figure 4.1-A,E). Therefore, a bias voltage up to several volts is required before electrons from the metal can resonantly flow through a molecular level ('resonant tunnelling'). Generally, such voltages result in huge electric fields, $> 10^9$ V/m, causing breakdown before the molecular level is actually accessed. Recently, Beebe *et al.* found a creative way out of this dilemma [5, 6]. They state that the position of the nearest molecular level in a two-terminal device can be derived from I-V (current-voltage) measurements, even if the bias voltage is moderate and resonance is not yet reached. All that is needed is to replot of the I-V data in a form that is based on the physics of field emission. Due to its simplicity and elegance, this method, coined 'transition voltage spectroscopy' (TVS), is becoming a very popular tool in molecular electronics [7–11]. However, a basic justification is still lacking. This chapter is therefore devoted to the physical interpretation of TVS. Beebe *et al.* employ the Simmons model for tunnelling to interpret their data and justify TVS [12]. Surprisingly, we find that the experimental results they present are not at all in agreement with this model. We show that a coherent molecular transport model, however, does justify their approach. Additionally we perform measurements on vacuum tunnel junctions to validate our predictions experimentally. Finally we critically evaluate this technique as a spectroscopic tool.

To introduce TVS, we initially follow the approach by Beebe *et al.*. They

make the analogy between molecular charge transport and electron tunneling through a rectangular barrier, as described by Simmons (see figure 4.1A-D) [12, 13]. Within this framework, the height of the tunnel barrier, ϕ, equals the energy offset between E_F and the nearest molecular orbital. For thiol-terminated molecules, the nearest level is commonly the highest occupied molecular orbital (HOMO, with energy E_{HOMO}), so that $\phi = E_F - E_{HOMO}$ (hole transport) [5, 6, 14]. The barrier width, d, is set equal to the length of the molecule. Simmons showed that for bias voltages $V < \phi/e$ with e the electron charge, the effective tunnel barrier is lowered to $\phi - eV/2$ (see figure 4.1C). However, for high biases, $V > \phi/e$, the barrier shape becomes triangular and part of the barrier becomes classically available. This case is generally referred to as Fowler-Nordheim tunnelling (FN) or field emission [15]. Figure 4.1D illustrates the transition between both regimes, at $V = \phi/e$. In the FN-regime, I is related to V by $I \propto V^2 exp(c/V)$, where $c < 0$ depends on the thickness and height of the barrier. Hence, plots of $ln(I/V^2)$ versus 1/V (FN-plots) yield a straight line with a negative slope, provided $V > \phi/e$. Beebe *et al.* took the approach to extend this way of plotting I-V data to low V. Interestingly, such FN-plots yield a well-defined minimum, at a voltage V_m. Intuitively, the existence of this minimum is easily understood. Since $I \propto V$ at low biases ($V \ll \phi/e$), an FN-plot of $ln(I/V^2) \propto ln(1/V)$ vs $1/V$ must yield a positive slope at low V (high $1/V$). At high biases, in the field emission regime, the slope is negative and thus a minimum appears in between. In fact, any I(V)-curve that evolves from linear to more than quadratic will have a minimum in a FN plot. Actually this is true for all the representations of the I-V characteristics of the form: $ln(I/V^\alpha)$ vs $1/V$ with $\alpha > 1$ [16]. Indeed for every α a minimum can be found, nevertheless we will concentrate in this chapter on the $\alpha = 2$ case.

Referring to the Simmons model, Beebe *et al.* suggest that: (i) V_m scales linearly with $\phi = E_F - E_{HOMO}$ (or $E_{LUMO} - E_F$, whichever level is closest); (ii) V_m is independent of molecular length d for constant ϕ; (iii) V_m equals the voltage at which there is a transition to the FN regime (hence 'transition voltage', see figure 4.1D) [5, 6]. Their striking experimental results substantiate these propositions. Measurements on self-assembled monolayers (SAMs) of a variety of conjugated molecules show that $V_m \propto E_F - E_{HOMO}$, where the latter difference is determined by photoelectron spectroscopy. Furthermore, they find V_m to be independent of molecular length, d, for alkanethiols. This is consistent with the fact that the HOMO-LUMO gap of these molecules is virtually length independent [6]. All these important observations make a strong case for TVS to become a general technique in molecular electronics.

We therefore start our study by investigating the Simmons model, put forward by Beebe *et al.*, in detail. Surprisingly, we find that it is in strong dis-

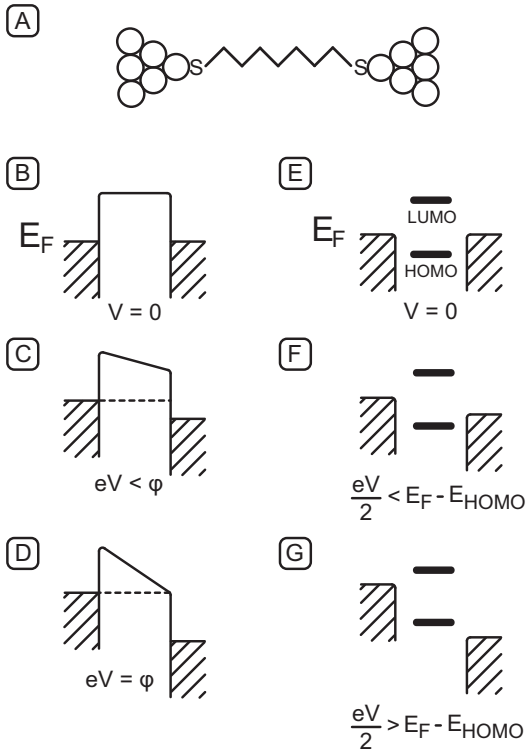

FIGURE 4.1: **Modeling a molecular junction. A** Molecular junction (thiol bonds). **B-D** Simmons model. Here, a molecule is depicted as a tunnel barrier of height ϕ and length d (**B**, for clarity we picture electron tunnelling only). Upon applying a bias voltage, the barrier is tilted (**C**). When $eV \geq \phi$, the barrier becomes triangular and electrons tunnel by field emission (**D**). **E-G**: resonant molecular model. Here, the molecular levels are broadened by the interaction with the electrodes (**E**). At elevated biases, the left and right chemical potentials open a window for transport of size eV (**F**). The current increases dramatically when a level is within the bias window (**G**, resonant tunnelling).

agreement with the experimental data in Refs. [5, 6]. To demonstrate this, we first make use of a simple, but rather accurate analytical model for tunnelling. This has the advantage that we can obtain a simple analytical expression for V_m. Subsequently, we confirm this result by using the full Simmons model numerically.

4.2 The Simmons model

To describe electron tunnelling in an elegant manner, we use a reformulation of Stratton's formula for direct tunnelling [17, 18]. This gives I(V)-curves of the form:

$$I \propto sinh(\frac{eV\tau}{\hbar}) \tag{4.1}$$

Here, $\tau = d\sqrt{m/2\phi}$ is the tunnel traversal time and m is the electron mass. Previously, a comparison between Simmons and Stratton was made by Hartman [19]. Due to the simple form of eq. 4.1, it is straightforward to determine an analytical expression for V_m. To find V_m, we put the derivative in a Fowler-Nordheim plot to zero. Substituting $y = 1/V$, we require:

$$\frac{dln(I/V^2)}{d1/V} = \frac{d}{dy}(ln(sinh(\frac{e\tau}{y\hbar})) + 2ln(y)) \tag{4.2}$$

$$= \frac{2}{y} - \frac{e\tau}{\hbar}\frac{1}{y^2}coth(\frac{e\tau}{\hbar y}) = 0. \tag{4.3}$$

Thus:

$$y_m = \frac{e\tau}{2\hbar}coth(\frac{e\tau}{\hbar y_m}) \tag{4.4}$$

By re-substituting $y_m = 1/V_m$, equation 4.5 is obtained.

$$\frac{1}{V_m} = \frac{e\tau}{2\hbar}coth(\frac{eV_m\tau}{\hbar}) \tag{4.5}$$

It is very instructive to discuss an approximate solution to eq. 4.5. For this, let us assume that $eV_m >> \hbar/\tau$, such that $coth(eV_m\tau/\hbar) = 1$. Then:

$$V_m \approx \frac{2\hbar}{e\tau} = \frac{2\hbar}{e\sqrt{m}}\frac{\sqrt{2\phi}}{d} \tag{4.6}$$

Before we discuss eq. 4.6, we check its validity by substituting it back into eq. 4.5. This yields $coth(e\tau V_m/\hbar) = coth(2) = 1.037$, so that eq. 4.6 is accurate within a few per cent.

Equation 4.6 is remarkably different from the results Beebe *et al.* obtained: (i) V_m is not proportional to the barrier height, but to its square root; (ii) V_m is not independent of the molecular length d, but inversely proportional to it; (iii) there is no general correspondence between V_m and the transition voltage at which a tunnel barrier becomes triangular (depicted in figure 4.1D). The latter voltage equals ϕ/e, independent of d, whereas eq. 4.6 yields $V_m \propto 1/d$.
Clearly, the Stratton approach is only an approximation. Nevertheless, eq. 4.6 turns out to have more general validity. To show this, we turn to the actual Simmons model. In our calculations, we include the integrals that are neglected in Ref. [12] itself. This prevents unphysical results for short and low barriers, a common problem in tunneling analysis (see appendix B). We proceed our discussion in the light of the most elaborate and convincing result Beebe *et al.* present. They perform TVS on a series of alkanethiol molecules with lengths ranging from 9 to 24 Å and find V_m = 1.2 V, almost independent of molecular length. Since alkanes have become a benchmark system in experimental transport studies, they form a perfect test bed for our present study as well [2, 3, 6, 13, 14, 20–24]. There is general agreement that $\phi = E_F - E_{HOMO}$ hardly changes with alkane length. However, for its precise value different numbers can be found in literature, even in the well-studied case of Au-S coupling [3, 13, 14]. In the following, we use ϕ = 4 eV [13]. For generality, however, all calculations presented below have also been performed for values, ϕ = 2.14 eV, taken from Ref. [14], and ϕ = 3 eV (see appendix B). The inset of Fig. 4.2a shows an I(V)-curve for a rectangular barrier with ϕ = 4 eV and d=10 Å, computed by the Simmons expression for the intermediate regime ($eV < \phi$). The corresponding FN-plot (main panel in figure 4.2a), exhibits a clear minimum around V_m = 1.5 V< ϕ/e. Thus, we have the tools at hand to test eq. 4.6 for the Simmons model. In figure 4.2b, we show V_m vs. $\sqrt{\phi}$ for a virtual series of ϕ-values, assuming constant length d = 10 Å. As anticipated above, we see that $V_m \propto \sqrt{\phi}$. Next, we plot V_m for a series of lengths d, with ϕ = 4 eV (see Fig. 4.2-C, blue line). Indeed, we find that $V_m \propto 1/d$. In fact, the Simmons result deviates very little from the line obtained using the Stratton approach (black in figure 4.2-C). We conclude that eq. 4.6 approximately holds for the Simmons model as well. Most importantly, however, these calculations confirm that there is a large discrepancy between data and model, as presented for TVS thus far [5, 6]. Hence, a new interpretation of TVS is due. Two different approaches can be considered for this. The first is to extend the Simmons model to include the image potential. The influence of the latter is that the effective barrier height ϕ decreases considerably [12, 13]. Since this effect is larger for shorter molecules, this may locally cancel the length dependence in eq. 4.6. Alternatively, we will consider a coherent transport picture based on molecular levels, Lorentz-

broadened by coupling to the leads. In that case, the voltage is assumed to drop fully at both metal-molecule contacts. This is in strong contrast with any type of tunnelling model, where the voltage drops evenly over the junction (see figure 4.1).

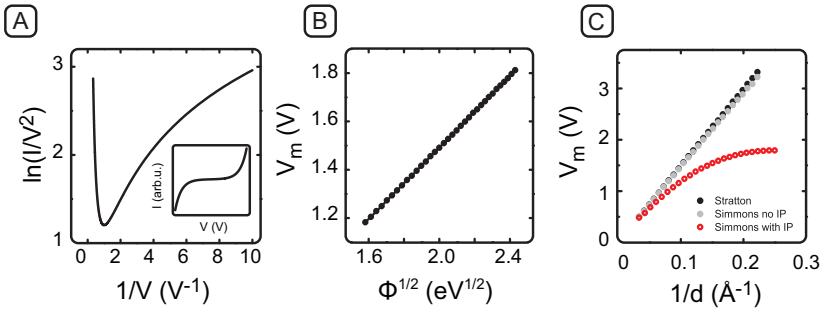

FIGURE 4.2: **Calculations on the length dependence of V_m according to Simmons.A**: Fowler-Nordheim plot for a barrier with ϕ=4eV and d= 10 Å, as predicted by the Simmons model. V_m is determined from the minimum of the graph. Inset: corresponding I(V)-curve on a linear scale. **B**: V_m versus $\sqrt{\phi}$ for the Simmons model (d=10 Å). The linear relation is consistent with eq. 4.6. **C**: V_m versus 1/d for $\phi = 4$ eV, using various tunnel models. Black: Stratton model (eq. 4.6). Light-gray: full Simmons model without image potential. Open circles: full Simmons model including image potential ($\epsilon_r = 2.1$). Clearly, V_m depends strongly on d in all cases.

For the calculations including the image potential, we used the full formulation of Simmons and eq. 35 of reference [12] with the correction of ref. [25] to calculate $\bar{\phi}$:

$$\bar{\phi} = \frac{1}{\Delta s}\int_{s_1}^{s_2}\{\phi_0 - \frac{eVx}{s} - \frac{1.15\lambda s^2}{x(s-x)}\}dx. \tag{4.7}$$

Here, $\lambda = e^2 ln2/8\pi\epsilon_r s$. For the local dielectric constant, we take $\epsilon_r = 2.1$ [26, 27]. s_1 and s_2 are the positions where the barrier is equal to the Fermi energy of the metal and were found numerically. Figure 4.2-C shows V_m as a function of $1/d$ (red line). For large d (small $1/d$), this result deviates little from the bare Simmons result. For smaller d, however, it differs considerably. In fact, a maximum in $V_m(d)$ is seen for larger values of $1/d$ than shown in figure 4.2-C, which indeed results from a decrease of the barrier height as the electrodes come closer to each other. Nevertheless, for the length scales that Beebe *et al.*

investigated (9 to 24 Å), V_m is still strongly dependent on d. Hence, we cannot explain the experimental data by including the image potential in a Simmons model. We note here that the Simmons model only presents a limited picture of tunnel barriers as pointed out in reference [28]. Besides we elaborated on the Simmons model to follow the reasoning of Beebe *et al.* and conclude that the model they present does not match their experimental results at all.

4.3 A COHERENT, MOLECULAR LEVEL MODEL

Let us therefore consider a more common picture of a molecular junction, as sketched in Fig. 4.1-E-G [29–33]. The molecular levels are located below (occupied) and above (empty) the Fermi energy of the metal contacts. Within the coherent Landauer approach, transport through such a junction is described by a transmission function T(E) that depends explicitly on energy. This function is peaked around the molecular levels. In fact, it has been extensively shown that a Lorentzian provides a good description for the transmission around a single molecular level [29, 30, 33]. Resonant tunneling can be achieved by applying the proper gate voltage in three-terminal junctions. In two-terminal devices, however, resonant tunneling is only possible by opening a voltage window eV high enough for the molecular level to fall in between the left and right chemical potentials (see figure 4.1-G). As discussed above, a device typically breaks down before this point is reached. Here, we will assume that one molecular level (HOMO) dominates transport, as is often the case in molecular junctions [5, 6, 14]. Thus our model captures the most relevant physics needed for an analysis of TVS. For T(E), this yields:

$$T(E) = \frac{\eta(1-\eta)\Gamma^2}{\Gamma^2/4 + (E-\varepsilon)^2} \tag{4.8}$$

where $\varepsilon = E_{HOMO}$ (we set $E_F = 0$). Furthermore, $\Gamma = \Gamma_1 + \Gamma_2$ denotes the total energy broadening due to the coupling between metal and electrodes. Specifically, $\Gamma_1 = \eta\Gamma$ and $\Gamma_2 = (1-\eta)\Gamma$ describe the overlap between the molecule and the left and right electrode, respectively. The parameter η denotes the asymmetry of the coupling. Symmetric coupling corresponds to $\eta = 0.5$. In that case, an applied voltage drops symmetrically at the left and right contacts (compare figures 4.1-D and 4.1-G). The I(V)-relationship can be calculated from the Landauer formula:

$$I = \frac{2e}{h}\int_{-\infty}^{\infty} T(E)[f_1(E) - f_2(E)]dE \tag{4.9}$$

Here, $f_{1,2}(E) = (exp((E-\mu_{1,2})/kT)+1)^{-1}$ is the Fermi function for a temperature T, at the left ($\mu_1 = eV/2$) and right ($\mu_2 = -eV/2$) electrode, respectively.

There is overwhelming experimental evidence that the zero-bias conductance of alkanes, as well as of many conjugated molecules, decreases exponentially with molecular length d. In general, one finds $dI/dV(V=0) \propto exp(-\beta d)$ where the decay constant β depends on the molecular series considered; β is highest for saturated molecules [1, 3, 34]. Interestingly, this result implies that also $T(E=E_F) \propto exp(-\beta d)$ (see eq.4.9). Indeed, several theory groups have confirmed such a relationship, using tight binding models in combination with (non-equilibrium) Green's function methods [31–33]. In our model, two free parameters exist, Γ and ε. In principle, both can depend on d. However, for longer alkanes, ε is known to be basically independent of d [13, 35]. Therefore, the length dependence must be in Γ. This has the immediate consequence that $\Gamma(d) \approx \frac{(E_F-\varepsilon)}{\sqrt{\eta(1-\eta)}} exp(-\beta d/2)$, using the fact that $E_F - \varepsilon >> \Gamma$ for longer alkanes. This relationship is consistent with extensive calculations by Samanta *et al.* for a series of oligophenyl molecules [33]. We note furthermore that Malen *et al.* applied a similar expression for $\Gamma(d)$ to successfully describe their experimental data [34]. Upon substituting $\Gamma(d)$ in eq. 4.8, a length dependent transmission function is obtained:

$$T(E,d) = \frac{1}{\frac{1}{4\eta(1-\eta)} + (\frac{E-\varepsilon}{E_F-\varepsilon})^2 exp(\beta d)} \tag{4.10}$$

Combining eqs. 4.9 and 4.10, we can calculate I(V)-curves for a series of molecular lengths and determine V_m. To compare to experimental data on alkanethiols, we take T= 300 K, $\varepsilon = -4$ eV and $\beta = 0.74$ Å^{-1} from extended literature [3]. Figure 4.3-A shows T(E) for several alkane lengths, whereas the inset of Fig. 4.3-B displays the corresponding FN plots. The length dependence of V_m is given in the main panel of Fig. 4.3-B. Remarkably, V_m is independent of molecular length for $d > 8$ Å. This is fully in agreement with the data of Beebe *et al.*, who find V_m to be independent of length for alkanes longer than 9 Å [6]. We note in addition that we find $V_m \propto \phi$ for a range of realistic values of ϕ (see figure 4.4).

We come to the important conclusion that TVS does indeed give us direct information on the molecular levels, as Beebe *et al.* have suggested. However, the interpretation of TVS only works within the framework of a coherent molecular transport model. Simmons-like pictures are inconsistent with experiments on molecular junctions.

4.4 Tunnel barrier or molecular levels?

Before we discuss further consequences of this conclusion, we take a critical look at figure 4.3. Despite the qualitative agreement, the value of V_m

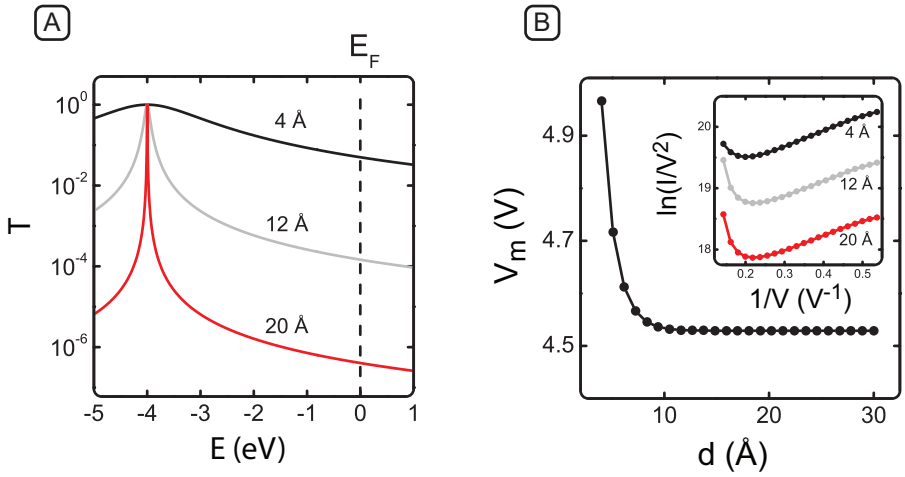

FIGURE 4.3: **Resonant molecular transport model applied to alkane junctions. A** Transmission function for three different lengths ($\varepsilon = -4$ eV, $T = 300$ K and $\beta = 0.74$Å [3]). **B** V_m versus molecular length d. V_m becomes length independent for $d > 8$ Å, consistent with the experiments by Beebe *et al.* [5, 6]. Inset: FN plots for the junctions in **A**.

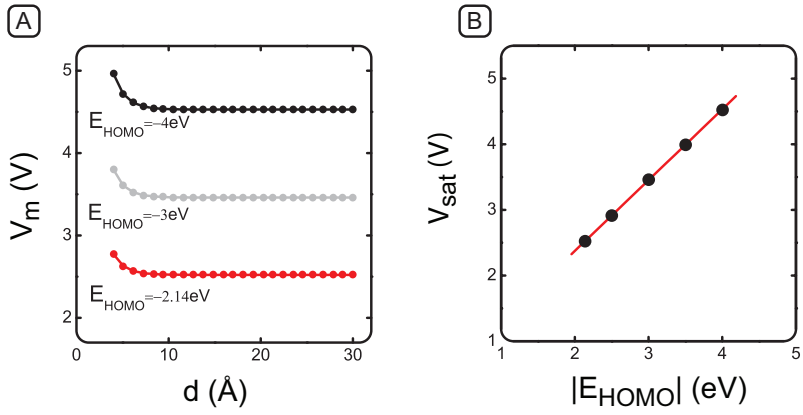

FIGURE 4.4: **Calculations on the length dependence of V_m for different E_{HOMO} values.A** V_m calculated using our coherent level model for several positions of the HOMO. For $d > 9$Å, V_m saturates to a value V_{sat} **B** Plot demonstrating that V_{sat} scales linearly with the position of the molecular HOMO level.

predicted by the model is much higher than found in experiment (though much lower than the resonant value $V = 2\phi/e$). This can have several reasons. First, $E_F - E_{HOMO}$ may be considerably smaller than 4 eV. As discussed above, there is quite some spread in the literature. Furthermore, the influence of image charges on molecular energy levels needs to be considered again. Just like in the Simmons case, the image force may yield a much lower level spacing for doubly contacted molecules as compared to free molecules. This phenomenon has recently attracted considerable theoretical attention [36–39]. Finally, although our Lorentzian model does capture the basic physics behind molecular transport, more detailed transport calculations will be needed to fully interpret TVS. Such studies should include the geometrical and electronic details of the molecular junction. For example, it was shown that the exact adsorption geometry of the molecule on the electrode has a pronounced effect on the shape of the transmission spectrum [14]. Recently, Mirjani *et al.* as well as Chen *et al.* presented in ref. [16, 40] a more detailed theoretical approach to the problem. Through their extended calculations they show, among other things, that our simple approach captures the essential physics involved. We will discuss this work in more details below.

To finalize our discussion, let us return to Figures 4.2 and 4.3. Clearly, the results for a coherent molecular model are radically different from those obtained for various Simmons models. There are two reasons for this. First, of course, the mathematics behind both models is not the same. Second, and perhaps more fundamental, the voltage profile is radically different. In the Simmons model, the potential decreases linearly with distance, whereas in the 'molecular' model, the voltage drops at the contacts only (see figure 4.1). It is easily visualized that the latter will result in a negligible length dependence of the shape of the I(V)-curves and thus in V_m being virtually independent of d. Interestingly, the very different properties of both models provide a fascinating perspective: TVS may allow us to distinguish molecular junctions (V_m independent of d) from tunnel junctions without molecules ($V_m \propto \frac{1}{d}$). Perhaps surprisingly, such a tool is still generally lacking in (two-terminal) molecular transport. As shown above, the data by Beebe *et al.* can only be understood within a 'molecular' model. Inversely, this can also be seen as evidence for the fact that they did indeed probe a molecular system. We note that such a distinction is not possible within the framework Beebe *et al.* present. If TVS in molecular junctions is explained by the Simmons model, there is no difference in the length dependence between a molecular junction with $E_F - E_{HOMO} = 4$ eV and a vacuum barrier with $\phi = 4$ eV, except in the image force via ϵ_r. Clearly, a tunnel junction without molecules will obey Simmons characteristics, resulting in $V_m(d, \phi)$ relations like in figure 4.2. To test this proposition, we performed a

series of experiments to consistently compare molecular junctions with tunnel junction for various lengths.

4.5 EXPERIMENTS ON VACUUM TUNNEL JUNCTIONS AND ORGANIC MOLECULES

Here we present extensive TVS measurements on: i) metal-vacuum-metal junctions[1] and ii) molecular junctions (more details in chapter 5) to test experimentally the propositions made above. Moreover we also include the results on molecular junctions from the literature.
In order to reveal the basic properties of TVS we need the possibility to accurately vary the tunnel gap between the electrodes. For a full characterization of TVS on a metal-vacuum-metal junction, voltages up to 3 V are to be applied over vacuum gaps as small as ≈0.3 nm. Such high electric fields (and high field gradients) may cause instabilities in the tunnel junctions. Hence, junctions are needed which are stable in time and kept in a clean environment. For this reason we used notched-wire mechanically controllable break junctions in cryogenic vacuum (T≈ 5 K) [41]. The electrodes are made of gold, the archetypical electrode metal for molecular junctions. In addition, the junctions were first optimized by a "training" procedure, i.e. by repeatedly opening and closing the electrodes [42]. We expect that this organizes the apex atoms into their strongest bond configuration and enhances their stability in high electric fields. The high stability and repeatability of the conductance evolution is illustrated by the tunnel curve in figure 4.5-A. Upon closing, the tunnel current increases exponentially until the electrodes snap to contact [42, 43]. Note that the conductance jumps to a value close to 1 G_0 ($1G_0 = 2e^2/h$), indicating a clean single-atom contact. After the training procedure, the electrodes are separated such that a vacuum gap is created with a zero bias conductance of ≈0.01 G_0. This is the starting point for the TVS measurements. Subsequently, the vacuum gap is increased stepwise, and an I-V curve over the range ±2-3 V is recorded for each position.

A typical example of such an I-V curve is plotted in figure 4.5-B. Clearly, the current displays a transition from a linear dependence at low voltages to a strongly nonlinear behavior for voltages $> 1.5V$. As stated earlier, this transition can be quantified by scaling the data in a Fowler-Nordheim representation. This is shown in figure 4.5-C, here for positive bias voltage only. Let us first discuss the upper curve. This curve is measured for a small tunnel gap with a

[1] The MCBJ vacuum tunnelling experiments have been performed by Marius Trouwborst and Tim Baart

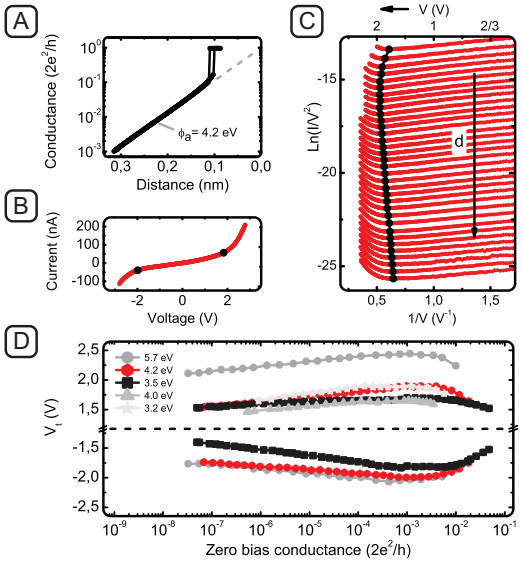

FIGURE 4.5: **Electrical characteristics of clean gold junctions at T≈ 5 K. A** Conductance versus width of the vacuum gap of a trained junction at a bias voltage of V = 100 mV. From the exponential decay at large distance, an apparent barrier height is deduced of 4.2 ± 1.0 eV (eq. 4.1) [44, 45]. **B** Typical I-V curve in the tunneling regime. Here, V_m is -1.99 V for negative voltage and 1.84 V for positive voltage (black dots), as obtained from: **C** Fowler-Nordheim plot of the I-V characteristics for 34 different positions. After each curve the electrode separation is increased by 0.02 nm, resulting in a lower current (no offset is used). The black dots represent the minima, or V_m. Remarkably, V_m decreases with distance for wide tunnel barriers while it increases for short tunnel barriers. **D** V_m versus zero bias conductance for different contacts, measured on 3 different samples. Note the break in the scale between -1.2 V and +1.2V. The two curves marked by triangles and stars are measured on the same sample, but the latter was obtained after modifying the electrodes. The same holds for the two curves marked by squares and hexagons. For each contact, the apparent barrier height was measured and its value is given next to the data points (± 1 eV).

zero bias conductance of ≈0.02 G_0. It has a well-defined minimum at 1.64 V that determines V_m. In total, 34 curves are plotted, corresponding to 34 different electrode separations (equally spaced by ≈0.02 nm). When we increase the electrode separation, a shift in V_m can be observed. The transition voltage first increases with distance and is at a maximum after stretching by ≈0.1 nm (fifth curve). V_m has now increased to 1.9 V. For even larger gaps V_m decreases again to a value of 1.55 V after stretching by ≈0.6 nm. In order to directly compare our measurements to the predictions of eq. 4.6, we need to plot the data as a function of $1/d$. For this purpose, the origin in the position ($d = 0$) was defined by extrapolating the exponential part of figure 4.5-A (dashed line) to a conductance of $2e^2/h$. The crossing point is then set as the origin. As a result we obtain figure 4.6. There is a striking difference when comparing the experimental data and the straight line expected from eq. 4.6: our data are not proportional to $1/d$. Instead, only a modest variation with d is found, with a maximum at ≈ 3 nm^{-1}. Clearly, the square barrier model (with a constant height ϕ) does not give an accurate description of the data. Qualitatively, the curves are very similar to the Simmons curves with image potential included, as shown in figure 4.2-C. However, we have to be careful not to apply this model quantitatively, since experimentally, we have atomically sharp electrodes. The Simmons model assumes two parallel plates. Let us first discuss the implications of our data for

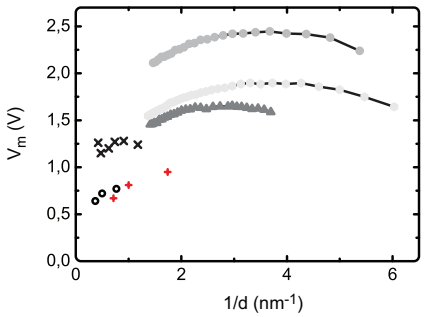

FIGURE 4.6: **Variation of the transition voltage with electrode distance.** Filled symbols: measurements of V_m vs $1/d$ for 3 different gold samples in vacuum. "×" and "+": data from large-area molecular junctions as reported by Beebe *et al.* "×": Alkane series, C_{18}-SH, C_{16}-SH, C_{12}-SH, C_{10}-SH, C_8-SH, and C_6-SH. "+": phenyl series, TP-SH, BP-SH, and Ph-SH [6]. "o": data presented in chapter 5 for OPEs of different length (OPE2DT, OPE3DT and OPE4DT) measured with C-AFM.

the interpretation of TVS. As described before, we want to make a comparison between the distance dependence of V_m for vacuum junctions and molecular

junctions. For this purpose, we also include three data sets measured by Beebe *et al.* and in chapter 5 in figure 4.6 [6]. The upper data set ("×"), corresponding to alkanethiols of different lengths, has a negligible variation in V_m. This was ascribed to an almost constant HOMO-LUMO gap for different alkane lengths. The lower data set ("+" and "o") corresponds to $\pi-$conjugated phenylene (from reference [6]) and phenylethynylene molecules (chapter 5) respectively. Compared to the alkanethiols, these molecules have a stronger dependence of V_m on d. This was attributed to a variation in the HOMO-LUMO gap, which is expected to decrease with increasing molecule length. Let us now compare the measurements. The two types of data (molecular junctions and vacuum junctions) have been measured at slightly different distances. In contrast to our MCBJ measurements, the experiments of Beebe *et al.* were carried out on large-area junctions, in which many molecules are probed in parallel. In addition, the distance between the Fermi level and the nearest molecular level is lower than the work function of the electrodes. As a result, the conductance is larger for the large-area molecular junctions which makes it possible to measure at larger distances or smaller values of $1/d$, respectively. Nevertheless, we find that the distance dependence of V_m for the molecular data does not differ significantly from that observed in our vacuum measurements. This is an important conclusion of this chapter. Taking into account (i) the measurement accuracy of the molecular data of approximately $\pm$100 mV and (ii) the limited variation of V_m with d for the vacuum data, it is not possible to distinguish molecular junctions from vacuum junctions just by measuring the distance dependence of V_m. However, considering the absolute values of V_m for conjugated molecules there is a clear difference with the vacuum data. For conjugated molecules, the reported values for V_m are much lower (0.6 V to 1 V) than the values found for the vacuum junctions (> 1.4 V) [16].

4.6 Does TVS have a future?

We mentioned in this chapter the possibility to use the distance dependence of V_m to discern molecular junctions from empty tunnel barrier junctions. Indeed we predict a $1/d$ dependence for a tunnel junction and a much shallower dependence for organic molecules. In contrast we show in our measurements on a tunnel barrier with a varying size, a length dependence that is strongly deviating from the predicted $1/d$ relation. The relation between V_m and the electrode separation d is somewhat similar for a tunnel barrier and a molecular junction. Hence it is difficult to make a distinction between those two types of junctions based on $V_m(d)$. What is striking here is the lack of agreement to describe a simple tunnel junction, although on the nanometer scale, with

standard models for tunnel barriers. Although, the Simmons model including images charges can describe the observed relation ($V_m(d)$) qualitatively, its intended use is for tunneling between two parallel plates and not for two sharp atomic sized electrodes. Here lies still a challenge for theoreticians.
In this chapter we identified several possible applications for TVS. Its original purpose is to access molecular levels without the need for the high voltages required for resonant tunneling. We show in this chapter that first of all TVS for molecular junctions can not be described by a tunnel barrier model like the Simmons model, as originally proposed by Beebe *et al.*. Nonetheless we can qualitatively reproduce the experimental results from reference [6] based on a simple resonant transport model. In this case it appears that indeed V_m is proportional to the position of the molecular level (HOMO or LUMO). Although this is confirmed by more elaborated calculations [16, 46, 47], this is the specific case of alkanethiols, where the HOMO/LUMO position is independent on the molecular length [3, 13, 14]. Unfortunately this approach is too simplistic for π-conjugated molecules, where the HOMO-LUMO gap decreases with molecular length [31, 33, 47]. So, to make a quantitative analysis of the molecular level positions, we need to take into account more parameters like the junction (a)symmetry, the number of levels involved and most importantly the potential profile of the junction[16, 47]. In our simple Lorentzian model we place the voltage drop at the contacts only and thus no voltage drop over the molecule itself is taking place, logically resulting in the distance independence observed. Mirjani *et al.* demonstrate with a more elaborated model [40] that the voltage drop over the molecule is crucial [47]. Their main result is presented in figure 4.7 where the value $\chi = |E_F - E_{level}|/V_m$ is plotted as a function of molecular length for the voltage dropping over the molecule and no voltage drop at all. The parameter χ is better suited than V_m to appreciate the performance of TVS. Indeed $E_F - E_{level}$ is dependent on the molecular length, χ circumvents this dependence. Here, in figure 4.7, we consider the two extreme cases, in reality the voltage drop is lying somewhere in between. i) When no voltage is dropping over the molecule, χ is rather constant. ii) When the voltage is dropping entirely over the molecule, we observe a clear dependence of χ on d. Though this is theoretically easily tuned, experimentally determining the exact potential profile over such a junction is quite challenging.

Moreover in order to explore the HOMO or LUMO level with TVS one must consider two unknowns, χ and the (a)symmetry [16, 47, 48]. The (a)symmetry can be determined experimentally out of the I(V) characteristics (see chapter 5). However χ remains experimentally difficult to access. Hence, TVS alone is not enough to explore the molecular energy levels without extra knowledge on the studied junction.

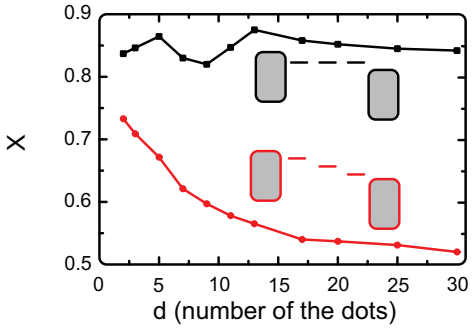

FIGURE 4.7: $\chi = |E_F - E_{level}|/V_m$ **versus the length of the molecule.** The calculations are done for the case where the voltage drop is only at the contacts (black squares) like schematically depicted in the higher inset and for the case the voltage drop is entirely over the molecule (circles) like shown in the lower inset. Taken from reference [47].

4.7 CONCLUSIONS

In this chapter we discussed a novel method for the analysis of current-voltage characteristics. Indeed transition voltage spectroscopy (TVS) held the promise of accessing molecular levels without the high voltages required just by replotting the I(V) curves as $ln(I/V^2)$ vs $1/V$ that will yield a minimum V_m. So V_m indicates the transition from a linear I(V) relation to a more than quadratic one, reducing the I(V) to a single number V_m.

We showed in this chapter that it is experimentally very challenging to extract information on the position of the molecular levels from TVS measurements. Indeed exact knowledge of both the junction symmetry and its potential profile are needed to relate the value of V_m to the energy of the HOMO (or LUMO). Experimentally we can deduce the symmetry of the junction from the I(V) curves, whereas determining the potential profile over a junction is still a challenge. At best a qualitative study of the molecular levels can be accomplished with TVS.

Moreover we demonstrated experimentally that V_m for a nanometer scale

tunnel junction behaves similarly to V_m for a molecular junction when varying the length of the junction. Nonetheless, the absolute value of V_m is lower for lower barriers or conjugated molecules. So it is not possible to unambiguously decide whether a junction is empty or populated by molecules, based on the value of V_m or its behaviour with length $V_m(d)$.

All in all, despite the appealing promises, TVS appears not to be an easily applicable tool for molecular electronics. Nonetheless it is still a potential system to test more advanced tunnel barrier models [28].

References

[1] N. J. Tao, *Electron transport in molecular junctions*, Nature Nanotechnology **1**, 173 (2006).

[2] S. Lindsay and M. Ratner, *Molecular Transport Junctions: Clearing Mists*, Advanced Materials **19**, 23 (2007).

[3] H. B. Akkerman and B. de Boer, *Electrical conduction through single molecules and self-assembled monolayers*, Journal Of Physics-Condensed Matter **20** (2008).

[4] M. S. Hybertsen, L. Venkataraman, J. E. Klare, A. CWhalley, M. L. Steigerwald, and C. Nuckolls, *Amine-linked single-molecule circuits: systematic trends across molecular families*, Journal Of Physics-Condensed Matter **20** (2008).

[5] J. M. Beebe, B. Kim, J. W. Gadzuk, C. D. Frisbie, and J. G. Kushmerick, *Transition from direct tunneling to field emission in metal-molecule-metal junctions*, Physical Review Letters **97** (2006).

[6] J. M. Beebe, B. Kim, C. D. Frisbie, and J. G. Kushmerick, *Measuring relative barrier heights in molecular electronic junctions with transition voltage spectroscopy*, ACS Nano **2**, 827 (2008).

[7] L. H. Yu, N. Gergel-Hackett, C. D. Zangmeister, C. A. Hacker, C. A. Richter, and J. G. Kushmerick, *Molecule-induced interface states dominate charge transport in Si-alkyl-metal junctions*, Journal of Physics: Condensed Matter **20**, 374114 (2008).

[8] K. Liu, G. R. Li, X. H. Wang, and F. S. Wang, *Length dependence of electron conduction for oligo(1,4-phenylene ethynylene)s: A conductive probe-atomic force microscopy investigation*, Journal of Physical Chemistry C **112**, 4342 (2008).

[9] B. F. C. Choi, S.H.; Kim, *Electrical Resistance of Long Conjugated Molecular Wires*, science **320**, 1482 (2008).

[10] G. Wang, T.-W. Kim, G. Jo, and T. Lee, *Enhancement of Field Emission Transport by Molecular Tilt Configuration in Metal-Molecule-Metal Junctions*, Journal of the American Chemical Society **131**, 5980 (2009).

[11] S. A. DiBenedetto, A. Facchetti, M. A. Ratner, and T. J. Marks, *Charge Conduction and Breakdown Mechanisms in Self-Assembled Nanodielectrics*, Journal of the American Chemical Society **131**, 7158 (2009).

[12] J. G. Simmons, *Generalized Formula For Electric Tunnel Effect Between Similar Electrodes Separated By A Thin Insulating Film*, Journal Of Applied Physics **34**, 1793 (1963).

[13] H. B. Akkerman, R. C. G. Naber, B. Jongbloed, P. A. van Hal, P. W. M. Blom, D. M. de Leeuw, and B. de Boer, *Electron tunneling through alkanedithiol self-assembled monolayers in large-area molecular junctions*, Proceedings Of The National Academy Of Sciences Of The United States Of America **104**, 11161 (2007).

[14] C. Li, I. Pobelov, T. Wandlowski, A. Bagrets, A. Arnold, and F. Evers, *Charge transport in single Au/alkanedithiol/Au junctions: coordination geometries and conformational degrees of freedom.*, Journal of the American Chemical Society **130**, 318 (2008).

[15] L. Fowler, R. H.; Nordheim, Proc. Roy. Soc. **119**, 173 (1928).

[16] J. Z. Chen, T. Markussen, and K. S. Thygesen, *Quantifying transition voltage spectroscopy of molecular junctions: Ab initio calculations*, Physical Review B **82**, 121412 (2010).

[17] R. Stratton, *Volt-current Characteristics For Tunneling Through Insulating Films*, Journal of Physics and Chemistry of Solids **23**, 1177 (1962).

[18] A. Bezryadin, C. Dekker, and G. Schmid, *Electrostatic trapping of single conducting nanoparticles between nanoelectrodes*, Applied Physics Letters **71**, 1273 (1997).

[19] T. Hartman, *Tunneling through asymmetric barriers*, Journal of Applied Physics **35**, 3283 (1964).

[20] W. Haiss, S. Martin, L. E. Scullion, L. Bouffier, S. J. Higgins, and R. J. Nichols, *Anomalous length and voltage dependence of single molecule conductance*, Physical Chemistry Chemical Physics **11**, 10831 (2009).

[21] L. Venkataraman, J. E. Klare, C. Nuckolls, M. S. Hybertsen, and M. L. Steigerwald, *Dependence of single-molecule junction conductance on molecular conformation*, Nature **442**, 904 (2006).

[22] M. T. Gonzalez, S. M. Wu, R. Huber, S. J. van der Molen, C. Schonenberger, and M. Calame, *Electrical conductance of molecular junctions by a robust statistical analysis*, Nano Letters **6**, 2238 (2006).

[23] C. A. Martin, D. Ding, H. S. J. van der Zant, and J. M. van Ruitenbeek, *Lithographic mechanical break junctions for single-molecule measurements in vacuum: possibilities and limitations*, New Journal of Physics **10**, 065008 (2008).

[24] E. H. Huisman, M. L. Trouwborst, F. L. Bakker, B. de Boer, B. J. van Wees, and S. J. van der Molen, *Stabilizing Single Atom Contacts by Molecular Bridge Formation*, Nano Letters **8**, 3381 (2008).

[25] J. G. Simmons, *Potential Barriers and EmissionLimited Current Flow Between Closely Spaced Parallel Metal Electrodes*, Journal Of Applied Physics **34**, 2472 (1964).

[26] B. de Boer, H. Meng, D. F. Perepichka, J. Zheng, M. M. Frank, Y. J. Chabal, and Z. Bao, *Synthesis and Characterization of Conjugated Mono- and Dithiol Oligomers and Characterization of Their Self-Assembled Monolayers*, Langmuir **19**, 4272 (2003).

[27] L. Bernard, Y. Kamdzhilov, M. Calame, S. J. van der Molen, J. Liao, and C. Schönenberger, *Spectroscopy of Molecular Junction Networks Obtained by Place Exchange in 2D Nanoparticle Arrays*, journal of physical chemistry C **111**, 18445 (2007).

[28] I. Baldea and H. Koppel, *Transition voltage spectroscopy: a challenge for vacuum tunneling models at nanoscale*, arXiv:1107.3501v1 [cond-mat.mes-hall] (2011).

[29] M. Paulsson and S. Datta, *Thermoelectric effect in molecular electronics*, Physical Review B **67**, 241403 (2003).

[30] J. M. Thijssen and H. S. J. Van der Zant, *Charge transport and single-electron effects in nanoscale systems*, Physica Status Solidi B-Basic Solid State Physics **245**, 1455 (2008).

[31] M. R. M. Mujica, V.; Kemp, *Electron conduction in molecular wires. II. application to scanning tunneling microscopy*, J. Chem. Phys. **101**, 6856 (1994).

[32] C. Joachim and J. F. Vinuesa, *Length dependence of the electronic transparence (conductance) of a molecular wire*, Europhysics Letters **33**, 635 (1996).

[33] M. P. Samanta, W. Tian, S. Datta, J. I. Henderson, and C. P. Kubiak, *Electronic conduction through organic molecules*, Physical Review B **53**, R7626 (1996).

[34] J. A. Malen, P. Doak, K. Baheti, T. D. Tilley, R. A. Segalman, and A. Majumdar, *Identifying the Length Dependence of Orbital Alignment and Contact Coupling in Molecular Heterojunctions*, Nano Letters **9**, 1164 (2009).

[35] D. M. Alloway, M. Hofmann, D. L. Smith, N. E. Gruhn, A. L. Graham, R. Colorado, V. H. Wysocki, T. R. Lee, P. A. Lee, and N. R. Armstrong, *Interface Dipoles Arising from Self-Assembled Monolayers on Gold UV Photoemission Studies of Alkanethiols and Partially Fluorinated Alkanethiols*, The Journal of Physical Chemistry B **107**, 11690 (2003).

[36] K. Kaasbjerg and K. Flensberg, *Strong Polarization-Induced Reduction of Addition Energies in Single-Molecule Nanojunctions*, Nano Letters **8**, 3809 (2008).

[37] J. D. Sau, J. B. Neaton, H. J. Choi, S. G. Louie, and M. L. Cohen, *Electronic energy levels of weakly coupled nanostructures C(60)-metal interfaces*, Physical Review Letters **101**, 026804 (2008).

[38] P. Hedegård and T. Bjørnholm, *Charge transport through image charged stabilized states in a single molecule single electron transistor device*, Chemical Physics **319**, 350 (2005).

[39] K. S. Thygesen and A. Rubio, *Renormalization of Molecular Quasiparticle Levels at Metal-Molecule Interfaces Trends across Binding Regimes*, Physical Review Letters **102**, 046802 (2009).

[40] F. Mirjani and J. M. Thijssen, *Density functional theory based many-body analysis of electron transport through molecules*, Physical Review B **83**, 035415 (2011).

[41] N. Agrait, A. L. Yeyati, and J. M. van Ruitenbeek, *Quantum properties of atomic-sized conductors*, Physics Reports-Review Section Of Physics Letters **377**, 81 (2003).

[42] M. L. Trouwborst, E. H. Huisman, F. L. Bakker, S. J. van der Molen, and B. J. van Wees, *Single Atom Adhesion in Optimized Gold Nanojunctions*, Physical Review Letters **100**, 175502 (2008).

[43] C. Untiedt, M. J. Caturla, M. R. Calvo, J. J. Palacios, R. C. Segers, and J. M. van Ruitenbeek, *Formation of a Metallic Contact: Jump to Contact Revisited*, Physical Review Letters **98**, 206801 (2007).

[44] A. Yanson, G. Rubio Bollinger, H. van den Brom, N. Agraït, and J. van Ruitenbeek, Nature **395**, 783 (1998).

[45] C. Untiedt, A. Yanson, R. Grande, G. Rubio-Bollinger, N. Agrait, S. Vieira, and J. van Ruitenbeek, *Calibration of the length of a chain of single gold atoms*, Physical Review B **66** (2002).

[46] M. Araidai and M. Tsukada, *Theoretical calculations of electron transport in molecular junctions: Inflection behavior in Fowler-Nordheim plot and its origin*, Physical Review B **81**, 235114 (2010).

[47] F. Mirjani, J. M. Thijssen, and S. J. van der Molen, *Advantages and limitations of transition voltage spectroscopy: A theoretical analysis*, Physical Review B **84**, 115402 (2011).

[48] T. Markussen, J. Chen, and K. S. Thygesen, *Improving transition voltage spectroscopy of molecular junctions*, Physical Review B **83**, 155407 (2011).